Cellular imaging with secondary ion mass spectrometry†

John S. Fletcher*

First published as an Advance Article on the web 24th September 2009
DOI: 10.1039/b913575h

This article is a concise review of the application of secondary ion mass spectrometry (SIMS) to the imaging of biological cells. The paper covers the various advantages and disadvantages of different approaches to SIMS analysis with respect to the information that can be gained from the interrogation of the cells. Current successes, pitfalls and future potential for SIMS in cell imaging are discussed. Developments in instrumentation that create a synergy between the traditionally separate fields of *static* and *dynamic* SIMS with particular benefits for cellular imaging by mass spectrometry are also described. Additionally, sample preparation and handling, and data manipulation and visualisation in SIMS are discussed.

Introduction

The invention and application of microscopy has revolutionised the way in which we visualise and understand cellular biology. Light microscopy, and equally ground-breaking electron microscopy, have dramatically increased our understanding of cellular composition and structure. Fluorescent markers have allowed cellular processes to be monitored and confocal methods can be used to generate 3D cell images. The ability to extract localised chemical information without the requirement of suitable tags would provide a further leap in analytical ability. Spectroscopic methods are beginning to make an impact but they can lack chemical specificity in complex biological samples. Mass spectrometric imaging offers the possibility for sub-cellular, chemical-specific imaging without the need for fluorescent tags.

Secondary ion mass spectrometry (SIMS) is an ultra high vacuum technique that takes advantage of the fact that when a target is impacted by an ion beam, secondary particles are ejected (sputtered) and some (in practice, a frustratingly small portion!) of these secondary particles become ionised.[1] The advent of mass spectrometry thus allowed this secondary ion ejection process to be used to characterise solid sample surfaces. The technique has been applied to a wide range of applications from astrochemistry to zeolite analysis. The sputtering process can be extremely surface-sensitive, yielding information from the uppermost atomic layers of a sample and the primary ion beams can be focused to spot sizes of tens of nanometres. The application to the analysis of biological samples such as tissue sections and single cells presents a wide range of challenges in terms of imaging resolution, sensitivity, sample handling and data analysis. However, the potential benefits are significant and wide-reaching.

Manchester Interdisciplinary Biocentre, University of Manchester, Manchester, UK. E-mail: John.Fletcher@manchester.ac.uk; Tel: +44 (0) 161 306 4440

† Electronic supplementary information (ESI) available: schematics of the modified Q-Star and the J105 instrument. See DOI: 10.1039/b913575h

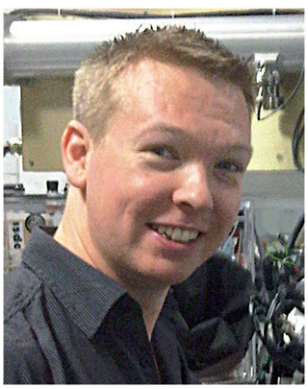

John Fletcher

John Fletcher received a Masters degree in Chemistry from UMIST before undertaking a PhD using ToF-SIMS and FTIR to characterise aerosols and thin film aerosol mimics. John is a PDRA at the University of Manchester. His research focuses on the development of new analytical approaches and novel instrumentation for the application of SIMS to the characterisation of biological materials including cells and tissue.

Dynamic SIMS

The first method developed for analysing samples with SIMS uses a high primary ion beam dose to erode the sample while analysing changes in composition as a function of depth. Due to its application in the semiconductor industry this method is still the most widely used. As the sample is constantly changing under the primary ion beam this mode of operation is termed *dynamic SIMS*. The dynamic SIMS instruments generally use a quadrupole or magnetic sector mass analyser. The first clear biological cell images were obtained using dynamic SIMS. Instrument manufacturer Cameca commercialised 'ion microscope' technology that allowed secondary ion images to be generated by extracting the secondary ions through a lens system similar to that used in an optical microscope. A large area of the sample (several hundred micrometres) is illuminated with a defocused primary ion beam and a selected secondary ion species is imaged. Unfortunately only one secondary ion species could be analysed at a time and the process was limited to atomic or very small fragment ions. The technique allowed the sub-cellular distribution of ions such as Ca^+ to be imaged in a range of plant and animal samples.[2]

Although limited to the imaging of either atomic or small fragment species the chemical microscope technique can be applied in many areas of research. The approach, dominated by

the work of Morrison and Chandra, has been used to map the distributions of both native species within cells and, to particular effect, the distribution of isotopically labelled additives. Levi-Setti *et al.* have gone even further and imaged halogen and isotopically enriched calcium in individual chromosomes.[3,4]

Zha *et al.*[5] and later Chandra and co-workers[6] have used ion microscopy to monitor the uptake of boron from boron neutron capture therapy (BNCT) drugs into different co-cultured cell types with relevance to therapies for cancer treatment. Such drugs provide an ideal candidate for demonstrating the power of chemical microscopy as they already incorporate a characteristic atomic marker – boron. Fig. 1 shows the distribution of boron, along with potassium and calcium in cells treated with sodium borocaptate (BSH). An optical image is also included that allows clear distinction to be made between the two different cell types in this example figure. A further level of sophistication was incorporated into the experiment where cells were co-treated with $^{13}C^{15}N$-labelled phenylalanine, to compare with the uptake and cellular distribution of the boronophenylalanine (BPA) drug. The SIMS imaging showed spatially resolved differences in the ratio of the boron from the BPA and the $^{13}C^{15}N^-$ despite the similarities of the two molecules. The BPA is a phenylalanine molecule with a $B(OH)_2$ moiety attached to the benzene ring. In particular, less intensity from the boron relative to the labelled phenylalanine was observed in the mitochondria-rich perinuclear cytoplasmic region, suggesting that mitochondria-associated cell processes may distinguish between the two similar molecules. Experiments were also performed to investigate the rate of uptake of the drug during different stages of the cell cycle. Cells were treated with the drug along with BrdU, a bromine-substituted uridine analogue that is incorporated into DNA during replication, during the s-phase of the cell cycle.[7] The nuclear region of cells in s-phase showed an increased uptake of boron when exposed to BPA for 1 h. The observation has particular potential relevance to brain tumour treatment where only the tumour cells would be expected to be proliferating and thus provide increased specificity in targeting cancerous cells by the drug. The work highlights how, despite the mass monitoring limitations, careful experimental design makes dynamic SIMS imaging an extremely powerful tool for pharmacology.

As more highly focused primary ion beams became available new methods for high spatial resolution imaging could be used. Microprobe imaging scans a highly focused ion beam across the sample and a mass spectrum is acquired at each point. Another development useful for cell imaging using dynamic SIMS was the implementation of parallel mass detection for a small number of species of pre-selected mass to charge ratio. Current commercial magnetic sector imaging SIMS instruments can now detect up to 7 species simultaneously.[8] The simultaneous mass detection has greatly improved the possibilities for the monitoring of isotopically labelled species since for accurate measurement and ratioing both the common isotope and the enriched label should be ejected from the same point at the same time. This method for SIMS analysis has been named multi-isotope imaging mass spectrometry, MIMS. A 2006 article by Lechene *et al.*[9] provides a comprehensive description of the technique with a wide range of cellular imaging examples, one of the most striking is reproduced in Fig. 2 and shows the distribution of $^{12}C^-$, $^{12}C^{14}N^-$ and $^{31}P^-$ in an endothelial cell.

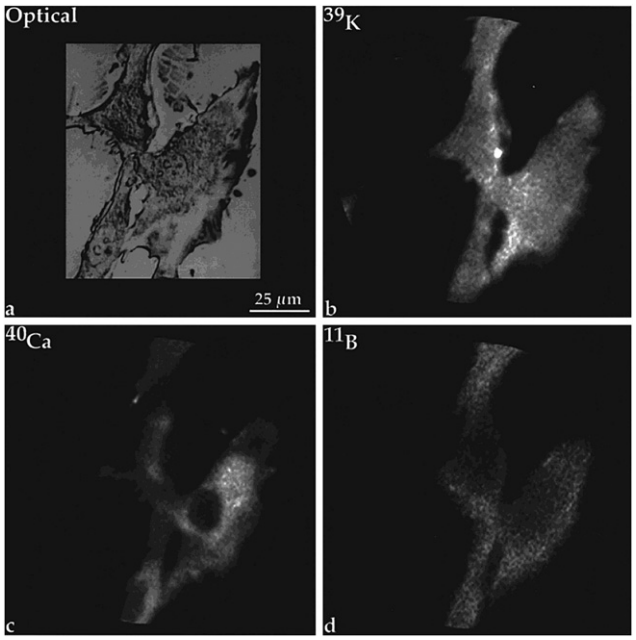

Fig. 1 Correlative reflected light Nomarski and SIMS imaging of a fractured, freeze-dried co-culture of T98G and GM3348 cells treated with BSH. (a) A GM3348 skin fibroblast is clearly recognizable at the right of the Nomarski image. (b–d) SIMS images of ^{39}K, ^{40}Ca, and ^{11}B from the same cells, respectively. (Reproduced with permission from ref. 6. Copyright 2001, Americal Chemical Society.)

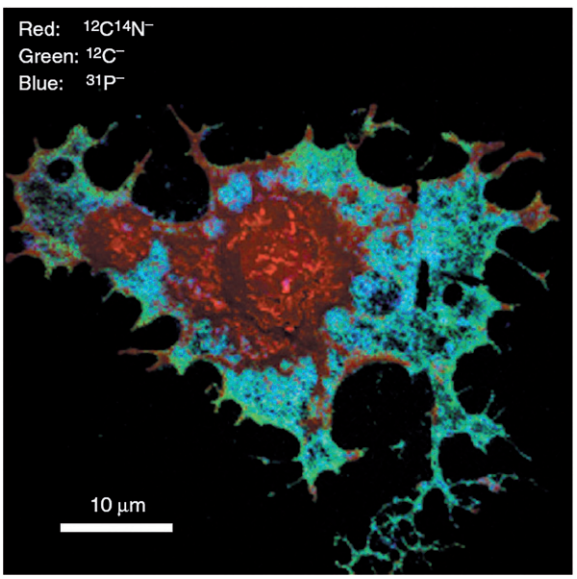

Fig. 2 Analysis of gross differences in composition within an unlabelled cell. Endothelial cells were cultured on silicon supports, fixed on the support, dried, and analysed with MIMS. Quantitative mass images of the surface of a whole endothelial cell were recorded in parallel at masses $^{12}C^-$, $^{12}C^{14}N^-$ and $^{31}P^-$. An overlay of these images is shown, with $^{12}C^{14}N$ in red, ^{12}C in green, and ^{31}P in blue. Scale bar = 10 μm. (Reproduced with permission from ref. 9. Copyright 2006, BioMed Central Ltd.)

Static/ToF-SIMS

Using conventional monoatomic primary ion beams, although including many 'small' cluster beams, the detection of intact molecular-type ions from the sample is limited to the uppermost layers of the material. This is due to the accumulation of ion beam-induced damage on the surface and in the sub-surface regions of the sample. Although the ejected material originates from the surface of the sample, the primary ion (or constituents of) actually penetrate and deposit their energy deep into the material. This results in disruption, including chemical bond breaking, of the sub-surface of the sample. If the same area of the sample is continuously analysed the signals from the sample change. The higher mass species are lost and the character of the spectrum tends towards elemental and small fragment ions. A limit is imposed due to the loss of molecular signal on the primary ion beam dose density that can be used and therefore on the amount of useful molecular information that can be extracted from the sample. This is generally referred to as the static limit and hence analysis within these conditions is termed *static SIMS*. For this method of analysis the time-of-flight (ToF) mass analyser has become ubiquitous due to the simultaneous detection of all ejected species, compared to scanning mass analysers, thus providing the high transmission required due to the constraints of the *static SIMS* experiment. Unlike the imaging magnetic sector instruments *a priori* knowledge of the sample, for target mass selection, is not necessary and therefore allows ToF-SIMS to be more easily employed as a discovery tool. In ToF-SIMS the analysis is almost exclusively performed in the microprobe mode, although the TRIFT instruments available from Physical Electronics Inc. have the potential to operate in a microscope mode and early proof-of-principle work to develop a suitable position-sensitive detector for biological imaging mass spectrometry has been reported by the Heeren group.[10]

There are, however, several drawbacks to the use of the ToF analyser due to the pulsed, cyclic nature of the experiment. Particularly in terms of instrument duty cycle and the need to generate very short (ns) primary ion beam pulses to maintain good mass resolution, that become exacerbated when the goal is the interrogation of single cells, these will be discussed later along with advances in instrumentation that are aimed to overcome these obstacles.

Despite the coupling of the ToF analyser to SIMS instruments in the 1980s there are few examples of the application of ToF-SIMS to cellular analysis until the mid-to-late 1990s.

The surface sensitivity of static SIMS makes the technique particularly suited to the analysis of the lipid membranes of cells. Several studies have been reported on the analysis of self-assembled lipid systems as cell membrane mimics to investigate the formation of different lipid domains.[11–13] Many of the ToF-SIMS studies of cells have focused on the identification and localisation of cell surface chemistry as opposed to the mapping of internal, atomic species using dynamic SIMS. One of the first reports of the ToF-SIMS imaging of single cells came from Winograd and Ewing at Penn State. *Paramecium*, single-celled organisms between ~180 and 310 μm long, were imaged using a Ga^+ liquid metal ion beam to investigate optimisation of freeze fracture conditions for ToF-SIMS analysis. The samples were also doped with either DMSO or cocaine hydrochloride following culturing.[14] The work provides a clear demonstration of the ability to use ToF-SIMS to analyse multiple organic fragments at sub-cellular resolution, although is must be noted that the signal levels for the organics within the *Paramecium* are extremely low with the cocaine signals only appearing to be slightly higher on the *Paramecium* than in the background, and the outline of the *Paramecium* is difficult to discern even by the more intense Na^+ and K^+ signals (Fig. 3). Also, in terms of biological interest it is physiological levels of drugs inside the cells which is a more interesting goal as opposed to artificially doped cells.

As mentioned, sensitivity to molecular species when performing high spatial resolution imaging was still severely limited. In order to increase secondary ion yield, some laboratories switched to In^+ primary ion beams where the more massive impacting ion helped improve the sputter yield. Ostrowski *et al.* describe the use of ToF-SIMS to image the changes in lipid composition during *Tetrahymena* mating using an In^+ primary ion beam.[15] During mating the *Tetrahymena* – common fresh water protozoa – form a series of highly curved fusion pores at the conjugation site that allow the passage of micronuclei between the cells. Such radical changes in the shape/structure of the membrane would be expected to involve a change in the lipid composition in that area. SIMS imaging of the *Tetrahymena* was performed following freeze fracture of the cells and inspection of the conjugation site, as hypothesised, showed a change in the lipid composition. A reduction in the signal from phosphocholine (*m*/*z* 184) was observed. Principal components analysis (PCA) was performed on the image and a species was identified at *m*/*z* 126 that was associated with the conjugation junction. The peak at *m*/*z* 126 was assigned to the headgroup of cone-shaped non-lamellar 2-aminoethylphosphonolipids (2-AEPs).

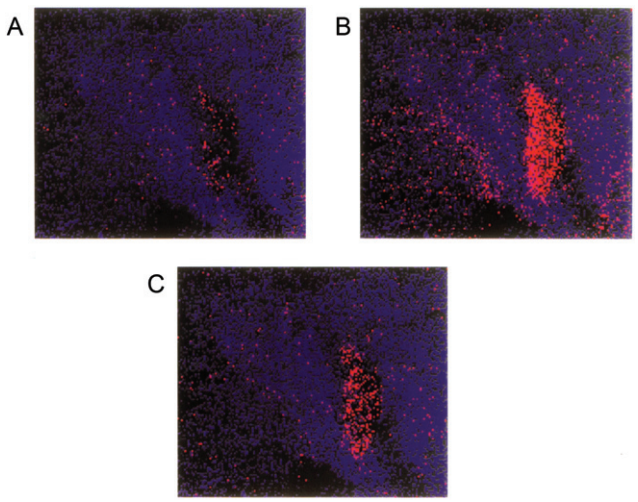

Fig. 3 ToF-SIMS images of a *Paramecium* sample previously exposed to a 10 μM cocaine solution. The cocaine image in (A) was produced by creating a two-colour overlay of the parent cocaine ion M + H with *m*/*z* 304 (the range of counts was 0–1) and a characteristic fragment *m*/*z* 105 (both in red) with water (blue). This image is compared to overlays of K^+ and Na^+ with water in (B) and (C), respectively. The field of view is 100 × 100 μm^2. (Reproduced from ref. 14. Copyright 1997, American Chemical Society.)

The localisation of such lipids at the conjugation site is consistent with the formation of the high curvature structures (Fig. 4).

The same group also performed studies to characterise freeze fracture sample preparation for ToF-SIMS[16] along with an investigation into the distribution of cholesterol in cell membranes.[17] Cells (a murine macrophages cell line, J774) were labelled with membrane-specific fluorescent tags (DiI, DiD) that were used to identify target cells for the SIMS analysis. As the cholesterol should be present in the cell membrane, only cells that had not lost their membrane during the freeze fracture sample preparation were selected for SIMS analysis based on the presence of the fluorescent tag. Cholesterol distribution was imaged using the characteristic $[M + H - H_2O]^+$ species present in the mass spectrum at *m/z* 369. The experiment was a success in that the cells were clearly identified by fluorescence in the vacuum system and cholesterol was detected in the sample. However, as can be seen from Fig. 5 the cholesterol signal levels, although localised to the cells, are still relatively low.

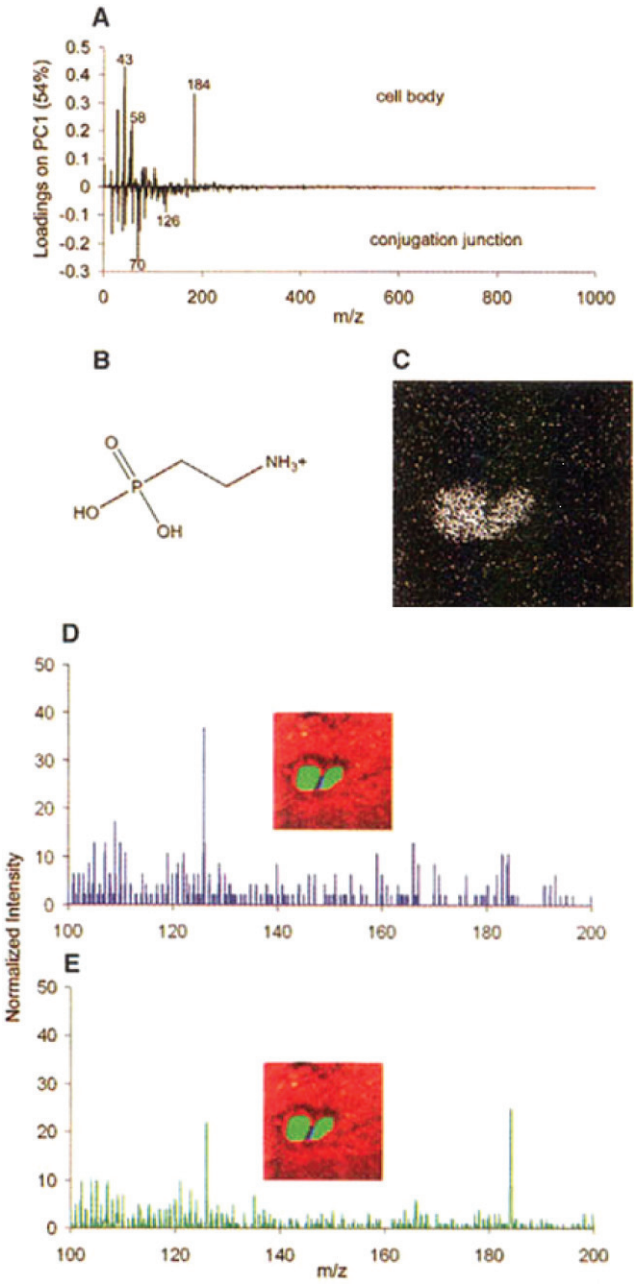

Fig. 4 The conjugation junction contains elevated amounts of 2-AEPs. Mass spectra from pixels were generated by selecting the pixels of interest using software written in-house. (A) Loadings plot from principal components analysis comparing the mass spectra of the cell bodies and the conjugation junction. (B) 2-AEP headgroup fragment corresponding to *m/z* 126. (C) SIMS image for *m/z* 126. (D) Mass spectrum from the pixels along the conjugation junction, as indicated in the inset. (E) Mass spectrum from the pixels in the cell bodies, as indicated in the inset. (Adapted from ref. 15. Copyright 2004, American Association for the Advancement of Science.)

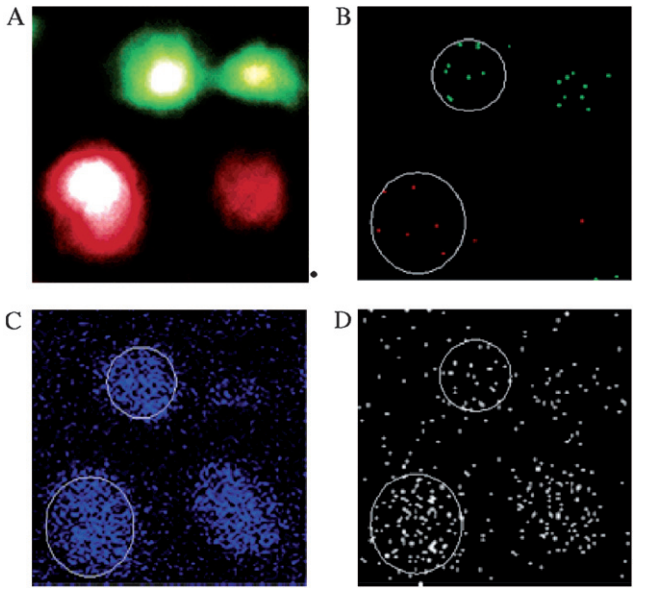

Fig. 5 Fluorescence and SIMS images of cholesterol-treated and control J774 cells (100 × 100 μm² field of view). Fluorescence and SIMS images were aligned manually using imaging software. (A) *In situ*, two-colour fluorescence image of several freeze-fractured J774 cells. The treated cells were arbitrarily coloured red, and the control cells are shown in green. (B–D) Positive ion molecule-specific images of J774 cells that correlate with the fluorescence image in (A). In all SIMS images, black pixels indicate an absence of signal. (B) SIMS composite image for DiD (*m/z* 860; red) and DiI (*m/z* 834; green). (C) SIMS image for $C_5H_9^+$ hydrocarbon (*m/z* 69; blue). (D) SIMS image for cholesterol (*m/z* 366–370; white). (Reproduced with permission from ref. 17. Copyright 2007, American Chemical Society.)

A number of methods exist for enhancing secondary ion generation in SIMS. Nygren *et al.*[18] and Sjövall *et al.*,[19] also aiming to image the lipid distributions in the cell, explored the use of silver printing. Silver foil was pressed against the cultured cell sample and the transferred material was imaged on the silver foil. The sputtered molecular species can appear as cationized molecular ions providing an increase in the ionisation efficiency and hence detected signal and image contrast. The studies demonstrated that Ag cationization could be used to localise cholesterol as $[M + Ag]^+$ with good effect (Fig. 6). In a further move towards direct cell analysis the same group later deposited a thin layer of silver onto cultured cells and then performed the SIMS analysis.[20] Again the Ag cationized cholesterol was observed with strong signal intensities. PCA was performed and

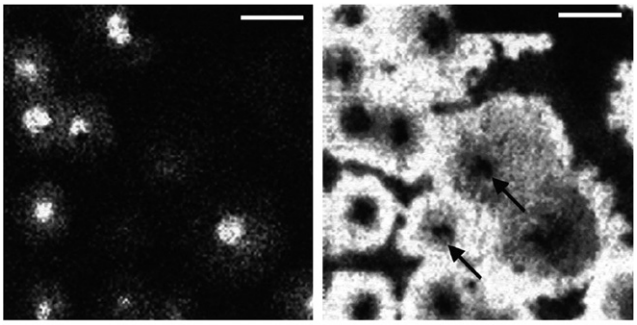

Fig. 6 Secondary ion images, *m/z* 184 (A) and 493 (B) obtained from silver imprints of glass-adhering leukocytes (polymorphonuclear leukocytes (PMNLs)). The cells were prepared by freeze-drying in ammonium formate. The scale represents relative intensity with white as maximum. Image area 100 × 100 μm^2; bar = 20 μm. Arrows indicate spots with low levels of ionisation. (Reproduced with permission from ref. 18. Copyright 2003, Elsevier.)

the nuclear and non-nuclear regions of the cell were distinguished.

The use of the cationization as a means of increasing secondary ion yield is clearly successful. However, as with any surface modification the silver printing and deposition may introduce further artefacts into the image. In the silver printing experiment the cholesterol is detected in the form of the silver adduct, *i.e.* as $[M + Ag]^+$ at *m/z* 493, with a significant enhancement in signal over cholesterol imaging in untreated samples, Fig. 6(B). The group also image the phosphocholine ion at *m/z* 184, Fig. 6(A). This peak is commonly observed in SIMS spectra of cells and tissue and is indicative of the polar headgroup from a number of membrane phospholipids. Silver cationization of this species is not observed as it is formed by a particular fragmentation and rearrangement of the lipid molecular ion that requires the addition of a proton and is thus not enhanced by the addition of the silver. In fact, the silver may actually be suppressing the signal from the *m/z* 184 fragment as it moves the molecular ion from the lipids into the $[M + Ag]^+$ channel. The lack of cholesterol signal in the nuclear region is surprising as the cell membrane should be covering the entire cell and thus, in a static SIMS experiment where only the surface layer is analysed, a continuous covering would be expected. Phosphocholine likewise should not be exclusively localised to the nuclear region and would be expected to be present in the same membranes as the cholesterol. With these considerations the work highlights both the advantages and potential complications arising from sample preparation/modification.

Similar to matrix assisted laser desorption ionisation (MALDI) mass spectrometry it is also possible to apply a matrix to the sample to enhance the secondary ion signal and this method is termed matrix enhanced (ME) SIMS. Altelaar *et al.*[21] and McDonnell *et al.*[22] have demonstrated the use of matrix application, 2,5-dihydroxybenzoic acid (2,5-DHB), to increase the high mass signal obtainable on a sub-cellular scale from the cerebral ganglia of *Lymnaea stagnalis*. Although the ultimate lateral resolution available may be reduced, due to the incorporation of the matrix, imaging is demonstrated with a lateral resolution of approximately 2.5 μm. However, as with the metal assisted SIMS the enhancement in secondary ion signal is not uniform across the mass spectrum and the authors observe a corresponding loss of the signal form the phosphocholine headgroup, *m/z* 184, when using the matrix as clearly illustrated in Fig. 7. The group more recently investigated the effect of gold coating the sample and gold coating the matrix-treated sample. Both the matrix addition and the metal coating showed enhancements, albeit with the same specificity reported above, and the combination of the two

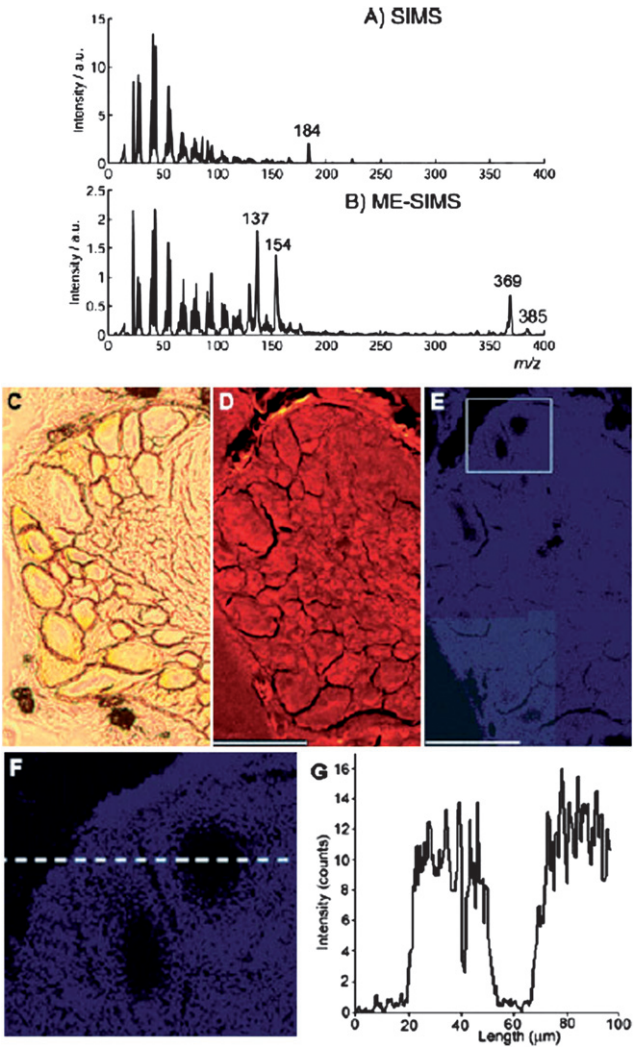

Fig. 7 ToF-SIMS spectra of a cerebral ganglion of the pond snail *L. stagnalis* (A) before and (B) after matrix deposition. (A) The SIMS spectrum only shows a peak at *m/z*, 184 corresponding to the phosphatidyl headgroup originating from phosphatidylcholine (PC) and sphingomyelin (SM), the two most abundant lipids in the plasma membrane. (B) In the ME-SIMS spectrum, clear signals at *m/z* 385 and 369 can be observed, corresponding to the $[M - H]^+$ and $[M - OH]^+$ molecular ions of cholesterol. (C) Light microscopy image of part of the parietal ganglion. (D) Total ion current (TIC) and (E) cholesterol (*m/z* 368.9–371.9) images of the same part of the parietal ganglion. The SIMS images were reconstructed from six separate measurements of 150 × 150 μm^2, with 10 μm overlap between two consecutive measurements. (F) A magnified image of the area highlighted in (E). A line scan was used to determine the experimental spatial resolution, 2.5 ± 0.2 μm. The position where the line scan was taken is indicated by the dashed line in (F) and the line scan is shown in (G). (Reproduced with permission from ref. 22. Copyright 2005, Wiley InterScience.)

methods showed no useful increase in signal compared to analysing the sample in its original, untreated state.[23]

Another method of increasing the secondary ion signal in ToF-SIMS is by laser post-ionisation (also sputtered neutral mass spectrometry, SNMS). As mentioned earlier, only a small portion of the material ejected in the sputtering process escapes in an ionised form. By firing a laser into the plume of sputtered material above the sample, prior to electrostatic extraction, the neutral species may become ionised and thus detectable by the mass spectrometer. Unfortunately the technique can be very specific in that there is as yet no global laser configuration that can ionise all species well. Atomic species provide easier targets as the laser can initiate fragmentation of many organic species. Hence the implementation of laser post-ionisation in SIMS has been limited to a small number of research groups. One particularly successful example of the method for sub-cellular imaging is, similar to Chandra with the chemical microscope,[6] the imaging of boron uptake for boron neutron capture therapy. The Arlinghaus group, following initial experiments using cell cultures,[24] has successfully imaged boron using SNMS in mouse kidney sections and in tumours implanted into nude mice where small fragments of lipids were also detected and imaged (Fig. 8).[25] A focused Ga^+ beam was used for the ejection of the secondary species and the sputtered boron was post-ionised using a focused excimer laser ($\lambda = 193$ nm, repetition rate = 200 Hz, pulse width = 20 ns, pulse energy = 100 mJ, spot size diameter = 150 μm).

A separate major leap in sensitivity was also gained by taking advantage of an effect that had been known for a number of years and this time providing an indiscriminate enhancement. This advancement came as a result of the development of new ion beams for SIMS analysis.

Dating back to the 1970s, a number of laboratories had observed a non-linear increase in the sputter yield from a sample as a function of increasing nuclearity of the primary particle.[26–28]

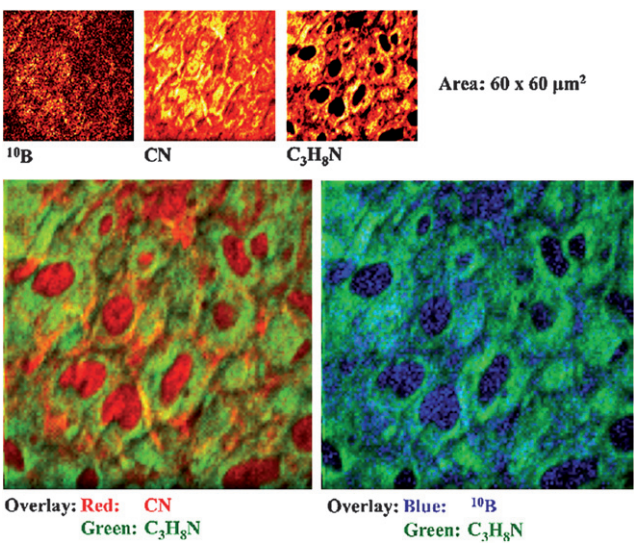

Fig. 8 Laser-SNMS images of a kidney sample from an NMRI nude mouse treated with a combination of BPA and BSH. C_3H_8N is a characteristic fragment of the phosphocholine headgroup. (Reproduced with permission from ref. 25. Copyright 2006, Elsevier.)

Experiments described by Blain *et al.* utilising primary particles of the type $(CsI)_nCs^+$, formed by the sputtering of a CsI target, resulted in several significant trends. Firstly the secondary ion yield increased with the mass of the primary projectile, and the secondary ion yield also increased linearly with the square of the velocity of the cluster projectile, *i.e.* proportional to the kinetic energy. Further, the secondary ion yield enhancement was greater for molecular secondary species compared with atomic secondary ions.[29,30]

Around the turn of the century, cluster liquid metal ion sources were introduced for routine SIMS analysis. Ion beams consisting of first gold[31] and later bismuth[32] clusters provided a significant enhancement in secondary ion yield and this increase was most significant in the higher mass range. The clearest example of this was the detection of the molecular ion from a sample of Gramicidin D using Au_3^+ where no signal was observable, even at considerably higher ion beam dose, using the conventional Ga^+ beam.

Arguably the greatest advance in the field of organic analysis with ToF-SIMS has been the implementation of polyatomic ion beams for routine analysis. Initial work from Appelhans and Delmore,[33] continued by Kotter and Benninghoven,[34] looking at methods for increasing secondary ion yields from polymers, reported that when the gas cluster ion SF_5^+ was used to analyse polymers there was not only the increase in secondary ion yield associated with the increase in mass, and the non-linear 'cluster effect', but also an increase in the amount of primary ion beam dose that could be used while maintaining characteristic molecular information. To paraphrase: the *static limit* could be relaxed. The group defined the efficiency of the ion beam as a ratio of the secondary ion yield to the disappearance cross-section of a given ion. Hence the most efficient ion beam would be one that produced a high secondary ion yield with the slowest decline of molecular information as a function of primary ion beam dose. Gillen and co-workers had also observed a similar effect with small carbon clusters.[35] The Vickerman group, in collaboration with Ionoptika Ltd., developed a C_{60}^+ ion beam system for routine analysis in SIMS. The ion beam produced a further increase in sputter yield, again with a greater effect on the higher mass region of the spectrum.[36,37]

A number of molecular dynamics simulations have been produced providing a comparison between the interaction of monoatomic species, small clusters and C_{60}^+ with the sample surface during the sputtering event. The monoatomic and small cluster ions such as Au_3^+ and/or Bi_3^+ penetrate the sample to a much greater depth than the C_{60}^+ ion, causing the disruption of many sub-surface layers with only a small proportion of the impact energy being transferred to the surface region of the sample and producing only a small yield of secondary particles. C_{60}^+, however, is expected to break up on impact and therefore is equivalent to the simultaneous impact of 60 carbon atoms each with 1/60th of the energy of the primary ion. The result is a massive ejection of material from the impact crater and, as each atom has only a relatively low energy, reduced disruption and damage of the sub-surface region.[38] The use of C_{60}^+ has allowed the static limit to be relaxed and in some cases ignored on a wide range of organic samples and has lead to the emergence of a whole new discipline in SIMS – *molecular* depth profiling.

In the area of cellular analysis the implementation of these ion beams has two implications. Firstly, the signal per pixel in an image can be increased by allowing analysis beyond the static limit and thus sampling a volume and, secondly, when sufficient signal is available 3D molecular imaging can be performed. Unlike a conventional depth profiling SIMS experiment the 3D analysis using a ToF analyser operates in a semi-dynamic mode where alternate analysis and etching cycles are performed. Although this approach is far from ideal, since precious potential signal is discarded during the etching periods of the experiment, it allows the analysis to be performed within a practical timeframe.

3D cellular imaging with SIMS

Chandra performed 3D single cell imaging using dynamic SIMS to generate a series of single mass images at increasing depths into a fractured freeze-dried T98G glioblastoma cell in the metaphase stage. The changing distribution of Ca^+ was observed as a function of depth.[39]

Fletcher *et al.*[40] demonstrated the initial application of ToF-SIMS using 40 keV C_{60}^+ ions to sputter etch and image *Xenopus laevis* oocytes, thus characterising chemical changes in three dimensions of a biological cell with minimal sample preparation/intervention. The *X. laevis* oocyte is a well-established cell model that has been extensively used in many branches of experimental biology and pharmacological research. It is a large single cell about 0.8–1.3 mm in diameter, the cellular compartments of which are so large that they are accessible to cell biologists for manipulation and visualisation. In addition, the *X. laevis* oocyte is remarkably resistant to osmotic changes. This facilitated the preparation of the cells for mass spectral imaging as they are reasonably resistant to washing of exogenous substances using de-ionised water. Although the handling of the sample was simplified due to the size of the specimen, the variation in topography over the analysis area resulted in reduced mass resolution and meant that over the course of the analysis only the outer section of the oocyte could be consumed. Despite this the sample provided clear proof-of-principle for molecular depth profiling of biological cells using C_{60}^+. Persistent secondary ion signals were observed through the analysis, where over 75 μm of material was eroded, for a range of species including cholesterol and diacylglycerides associated with previously identified, by extraction and MS analysis, lipid species known to be abundant in *X. laevis* oocyte membranes (Fig. 9).[41]

The C_{60}^+ beam, arising from a gas phase electron impact source, is inherently difficult to finely focus while maintaining enough current to enable analysis on a useful time scale. A compromise can therefore be used where a liquid metal ion beam is used to perform the imaging cycles of the experiment while a polyatomic ion beam is used for the interleaved etching periods to remove any damage generated by the LMIG beam. Breitenstein *et al.* employed this method of analysis for the 3D ToF-SIMS imaging of normal rat kidney (NRK) cells.[42] Bi_3^+ ions were used for the imaging while C_{60}^+ was used for the etching. The high spatial resolution imaging of the Bi_3^+ allows the sample to be imaged with sub-cellular resolution in 3D. Fig. 10 shows the cells clearly outlined against the substrate while the combination of amino acid-associated peaks also highlights the cells while the nuclear region can clearly be defined by the absence of pooled phospholipid signal. Although extremely impressive work it highlights a further compromise associated with high resolution ToF-SIMS imaging. The imaging was performed in a low mass resolution (*i.e.* using a longer than normal primary ion pulse) mode while a non-imaging high mass resolution mass spectrum must be acquired for accurate peak assignment. This is common with high resolution ToF-SIMS imaging where too rapid pulsing and/or bunching of the primary ion beam can prevent the realisation of the full focus of the ion beam, and the low ion currents from the focused and apertured ion guns mean that the experiment time becomes much longer so it is desirable to increase the amount of primary ions in each shot thus increasing the duty cycle of the experiment in terms of ion fluence over time. This mode of operation has a detrimental effect on the quality of the mass spectrum.

Sample handling

The high vacuum required for the optimum operation of the SIMS instruments presents a number of challenges in the handling of biological samples. Unlike electron microscopy, the distribution of chemical species, and not only the morphology, of the sample must be maintained. Chandra *et al.* routinely used freeze fracture and freeze-drying prior to SIMS analysis before moving towards frozen hydrated analysis.[43] The sample is placed between two pieces of silicon, or other suitable substrate, often accompanied with spacer beads of a similar (height) dimension to the cells in order to protect them from squashing. The sandwich is then plunged into a suitable cryogenic liquid, usually liquid nitrogen-cooled iso-pentane or propane, so that the sample freezes at a rate that prevents the formation of large ice crystals and hence redistribution of small molecules or possible rupturing of the cell. The frozen sandwich is then snapped apart exposing cells ready for analysis. Subsequently the sample is slowly dried under vacuum and analysed at room temperature. Combined electron microscope imaging and SIMS analysis has been used to verify the integrity of the sample following preparation. A K:Na ratio of approximately 10:1 is observed inside fractured cells. Alternatively, characteristic fragments from lipids present on the cell surface show membrane to be present and fluorescent tagging as shown in Fig. 5 can add extra clarification.

Alternatively, if suitable facilities are available in the SIMS instrument the sample may be fractured and then analysed in a frozen hydrated state. Although this method obviously adds to the level of experimental complexity it offers the best chance of observing the cell in a lifelike form. There are a number of further possible advantages to this method of analysis. One of them arises from the presence of the water as a matrix for the analytes of interest. The majority of molecular biological species observed in the ToF-SIMS spectrum appear as a result of proton transfer in the form $[M + H]^+$ or $[M - H]^-$. Conlan *et al.*[44] reported an increase in the yield of molecular ions, and characteristic fragments, of the amino acids alanine and arginine, and the nucleic base adenine in an ice matrix. A corresponding reduction in the ratio of protonated to non-protonated water cluster peaks in the mass spectrum (*i.e.* $(H_2O)_nH^+/(H_2O)_n^+$) was also observed suggesting that the water ice was providing a supply of protons to the organic molecules and promoting the formation of the molecular $[M + H]^+$ ions. Hence the analysis of frozen hydrated cells may lead to an increase in ionisation of biological species without the

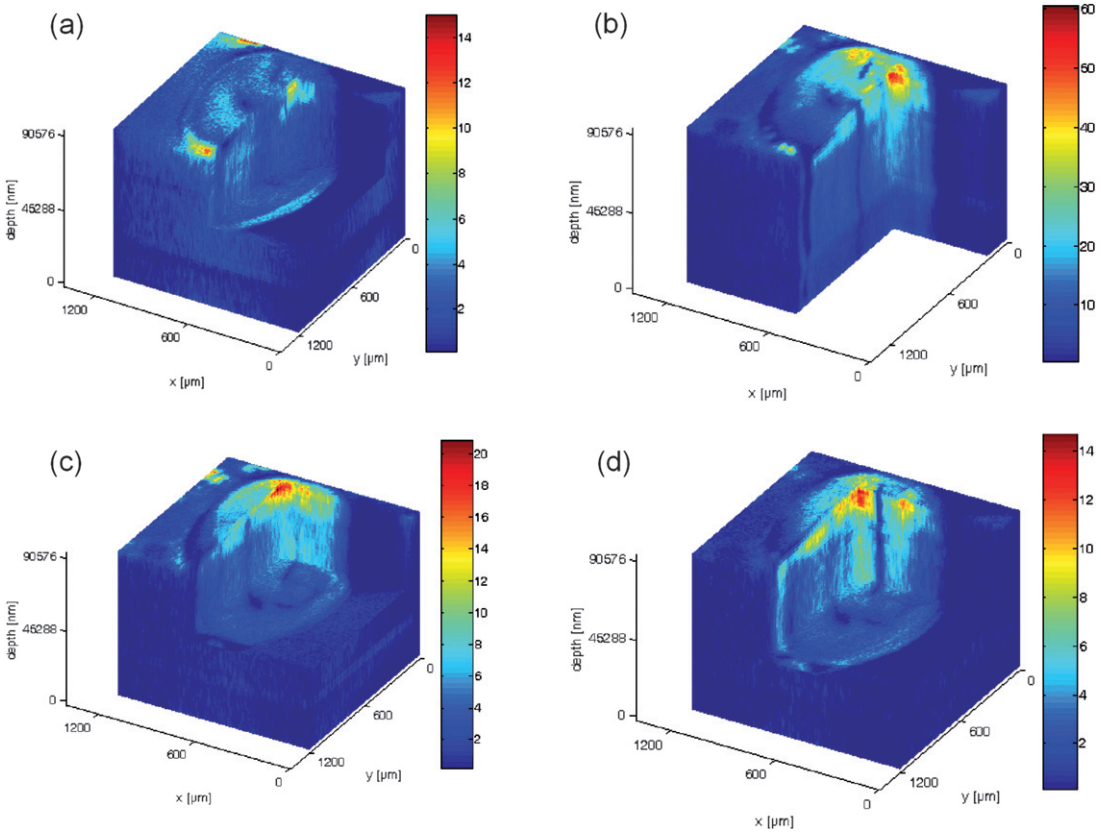

Fig. 9 3D biochemical images of freeze-dried oocyte, showing changes in (a) phosphocholine peaks *m/z* 58, 86, 166, and 184, (b) signal summed over the *m/z* range 540–650, (c) signal summed over the *m/z* range 815–960, and (d) cholesterol peak at *m/z* 369. Colour scale normalized for total counts per pixel for each variable (*m/z* range). (Reproduced with permission from ref. 40. Copyright 2007, American Chemical Society.)

complications, discussed previously, associated with metal assisted and matrix enhanced SIMS. Suppression or enhancement of a particular species in the mass spectrum based on its chemical environment (the matrix effect) can lead to misinterpretation of the image results and has been shown to follow a general trend of gas phase basicity. Again the excess protons may help to ameliorate this effect.[45] Preliminary work has shown some reduction of the matrix effect when condensing water onto a mixture of cytosine and 2,4,6-trihydroxyacetophenone (THAP) during SIMS analysis.[46] At present, however, there are insufficient data to draw a firm conclusion on the difference frozen hydrated conditions might have on biological sample analysis since many instruments are not equipped with the cryogenic sample handling facilities and the added experimental complexity makes the simple method of freeze-dried room temperature analysis much more seductive. Zheng *et al.* have also shown that when depth profiling model molecular systems, in this case two alternating Langmuir–Blodgett film layers, depth resolution is improved when performing the analysis at cryogenic temperatures.[47]

Another important issue, principally with molecular analysis and especially for depth profiling and 3D molecular imaging is that excess salts from the buffer solutions used during cell culture must be removed. The cells are usually washed in a medium that maintains osmotic pressure and thus prevents the cells from bursting. Wu and co-workers at Lawrence-Livermore examined a number of different washing techniques and found that ammonium acetate performed well as, due to its volatility, no residue remained and large numbers of cells were still able to proliferate following washing, thus proving preservation of biological integrity.[48] Interestingly, following washing to remove salts while maintaining cell integrity the group allow the cells to dry in air and thus leach out the cytoplasm. The cytoplasmic residue is then imaged around the cell at room temperature thus allowing internal chemistry associated with individual cells to be sampled without freeze fracturing or depth profiling. Ammonium formate washing[49] is also favoured by a number of groups, particularly Sjövall[19] and Nygren.[20]

Finally, chemical fixation can also be used. Although probably the most disruptive to the cell chemistry, chemical fixation is widely used in light microscopy, so for cross-comparison of data between the two imaging techniques it can be a valid method for sample preparation. Breitenstein *et al.*[50] have attempted to perform 3D SIMS imaging and 3D confocal microscopy on the same sample with some success. Care, however, must be taken when trying to infer biological information from species that do not show up in the microscopy and thus cannot be proved to have remained in their original state as it has been shown that chemical preparation may impair sub-cellular localisation compared to freeze preparation techniques.[51]

Developments in instrumentation

The desire to fully capitalise on the advantages delivered by polyatomic ion beams, coupled with the limitations in the

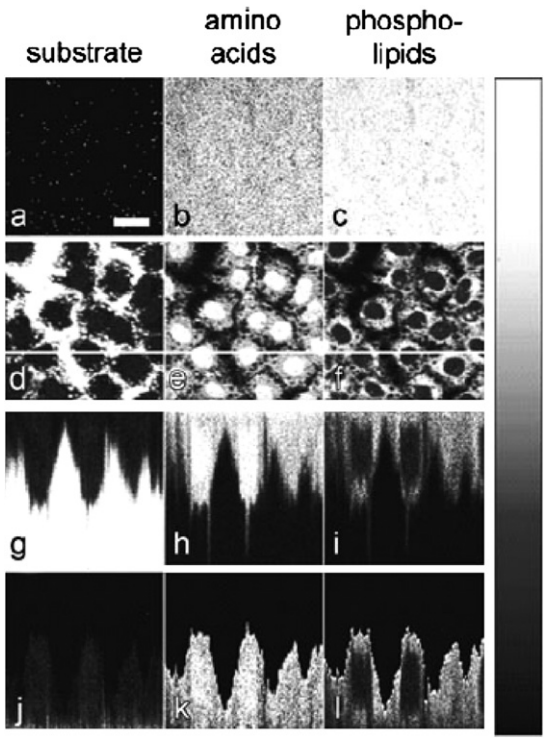

Fig. 10 Mass-resolved secondary ion images of the sample surface before any sputter cycle had been applied (a–c) and within the cell after the 45th sputter cycle (d–f). Image intensities are colour coded on a black-and-white scale with white corresponding to high intensities. The colour scale is normalized to the intensity in the brightest pixel. The scale bar in (a) corresponds to 20 μm. (g–i) *xz*-Sections through the three-dimensional data stack along the white line in (d)–(f). Parts (j–l) show the data of parts (g–i) after a mathematical correction of the *z* axis. Mass-resolved images are based on the following secondary ions: (a), (d), (g), (j): Na^+; (b), (e), (h), (k): amino acid fragment ions (pooled signal for masses 30 u, 44 u, 70 u, 101 u, 110 u, 136 u); (c), (f), (i), (l): phospholipid fragment ions (pooled signal for masses 58 u, 166 u, 184 u, 760 u). (Reproduced with permission from ref. 42. Copyright 2007, Wiley InterScience.)

application of conventional ToF instruments to these studies, have provided the impetus to develop new ways of applying SIMS to biological samples. Significant efforts have been directed towards this task by our laboratory and also by the Winograd group. The approaches may appear very different but have many fundamentally similar aspects. These similarities arise through both groups seeking to overcome the issues of duty cycle and spectral quality. Both of these can be overcome if the mass spectrometry can be decoupled form the sputtering aspect of the SIMS process.

The Winograd group has worked in collaboration with Applied Biosystems to modify the front end of a commercial MALDI platform (Applied Biosystems Q-Star XL) to allow the incorporation of a C_{60} ion beam system.[52]† Here the C_{60} beam is used instead of the laser of the MALDI instrument front end and is run either continuously or using extremely long pulses. A continuous stream of secondary ions is extracted by gas flow into the mass spectrometer where it passes through a series of quadrupoles prior to electrostatic push-out into an orthogonally mounted ToF analyser.

This development has definitively overcome the issues raised above in regards to spectral quality. The mass spectrometry is completely decoupled from the secondary ion generation process removing the contribution from the ion beam pulse length and topographic effects. The result is a secondary ion mass spectrometer with excellent mass resolution ($m/\Delta m \approx 14\,000$) in all modes of operation. The adaptation of the instrument allows complementary data to be obtained using the SIMS and MALDI modes of operation with the SIMS providing an improvement in the lateral resolution of the instrument. However, at present the capabilities for the very high spatial resolution imaging normally associated with SIMS are limited. On the prototype instrument the primary ion beam cannot be rastered and the instrument is only fitted with a course sample stage, making most single cell imaging impossible. If these technological drawbacks can be overcome the ultimate imaging resolution of the instrument is expected to be determined by the scattering of the primary ion beam by the relatively high (~1 Torr) gas pressures in the sample region of the instrument. Secondary ion transit times through the quadrupole system will also limit the rate of image acquisition as the beam cannot be moved to the next pixel until all ions from the current pixel have reached the detector.

The approach in our laboratory has been somewhat different in that we have chosen to work closely with manufacturers of ion guns and mass spectrometers to develop an instrument purpose-built for 2D and 3D SIMS imaging using novel methodology.[53]†

The resulting instrument, the J105 *3D Chemical Imager* (Ionoptika Ltd, Southampton), exploits a unique linear buncher in conjunction with a harmonic reflectron ToF analyser. As with the Q-Star platform, the instrument allows a continuous primary ion beam to be used for the analysis. The buncher, which is approximately 30 cm long, is filled with a portion of secondary ions. Next the buncher fires by suddenly applying an accelerating field that varies from 7 kV at the entrance of the buncher to 1 kV at the exit. This creates a time focus at the entrance of the ToF analyser as the ions from the back of the buncher catch up with those from the front.

The ultimate mass resolution is, like the Q-Star, decoupled from the sputtering event and is now dependent on the quality of this focus. Due to the acceleration in the buncher, the ions now have a 6 keV energy spread. A harmonic field ToF reflectron is required and employed such that the path of the ions is dependent only on the mass and charge, not the energy, of the secondary ions. The secondary ions undergo half a period of simple harmonic motion in the analyser before impacting the detector with the same time spread as the focus from the buncher.[54] The system is currently delivering $m/\Delta m \approx 6000$ at mass 500 although an upgraded buncher is to be installed shortly that is expected to produce in excess of $m/\Delta m > 10\,000$.

The sample handling and secondary ion generation and extraction of this instrument are more comparable to a conventional ToF-SIMS instrument than on the hybrid Q-Star instrument in that the design is based around an ultra high vacuum system and the secondary ions are extracted electrostatically. The sample handling is also optimised for manipulation of frozen biological specimens with insertion and analysis sample stages that can be cooled to liquid nitrogen temperatures and a glove box to prevent atmospheric water deposition during sample insertion. The instrument is thus able to fully exploit the high

resolution imaging available using focused ion beams while increasing the duty cycle and improving the quality of the mass spectra.

The duty cycle increase on the instruments described above allows depth profiling experiments to be performed without the interleaved analyse/etch protocol, thus maximising sensitivity and combining the speed of the dynamic SIMS instrumentation with the multiplexing advantage of the ToF analyser. In the case of the J105, high lateral resolution 3D imaging is possible in a manageable timeframe without the necessity for dual beam analysis and without discarding valuable material. The increase in acquisition rate associated with both instruments facilitates larger area imaging, for example, sectioned tissue samples.

Fig. 11 illustrates the possibilities available for cellular imaging using continuous (as opposed to pulsed) polyatomic ion beams. A reconstructed image of benign prostatic hyperplasia cells comprising 16 stacked images allows the biochemistry to be explored in 3D. Phospholipid signal is observed around a central area in which there is an abundance of signal from adenine expected to be particularly high in the nucleus. The data were acquired in a morning where it would have taken months to years to perform, without the aforementioned compromises, on a conventional ToF-SIMS instrument. Also shown in the figure are the distributions of the same ions in HeLa cells. These cell images, at higher lateral resolution, were acquired using the alternative approach of consuming all of the available material in a single image. The result is more comparable to what one would observe in a bright field microscope image or the type of images associated with dynamic SIMS although for molecular species. The adenine signal is highest in the nucleus although is seen extending out through the cell. The phospholipid signal highlights the cell membrane with particular intensity around the nucleus, most likely arising from the endoplasmic reticulum. Even though the pixel area is now only 1 μm, by analysing beyond the static limit, high signal levels are recorded; the maximum number of counts per pixel is 1886 for the adenine peak and 3789 for the phosphocholine signal (from a 0.1 amu mass channel).

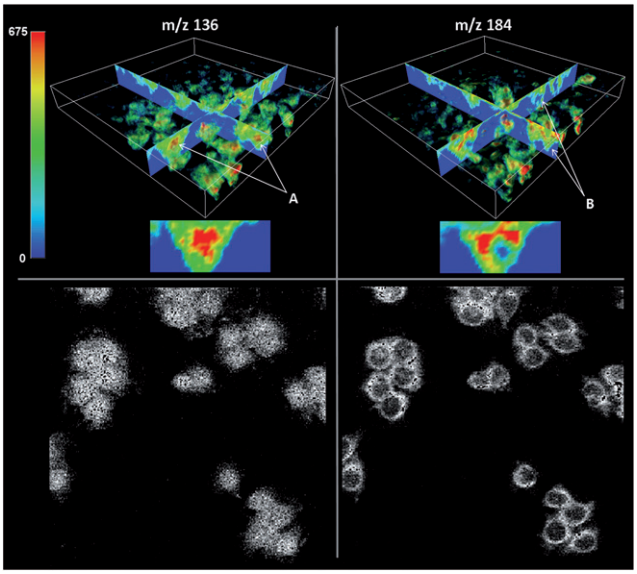

Fig. 11 Cell imaging using the J105. Top half of figure shows a 3D reconstruction of image data from BPH cells. Isosurface rendering shows the distribution of signal in 3D through the entire sample while orthogonal slices through the data set facilitate visualisation of the chemical distribution within selected cells. Data shown for the *m*/*z* 136 ion (left), the protonated molecular ion from adenine, and *m*/*z* 184 (right) originating from phosphocholine-containing lipids. The adenine signal is localised to the centre of the cells (A) as it arises from the nuclear DNA while the *m*/*z* 184 signal is observed almost as rings around the edge of the cell (B) as it arises from the lipid membrane. A larger view of the orthogonal slice through a single cell is also shown for clarity. Field of view for the analysis was approximately 180 × 180 μm, 128 × 128 pixels; 16 images were acquired as the analysis progressed through the cells. (Reproduced with permission from ref. 53. Copyright 2008, American Chemical Society.) Lower images are the same ions from a 256 × 256 μm, 256 × 256 pixel image of freeze-dried HeLa cells. In this analysis the entire sample was consumed in the generation of one image. Result is comparable to a bright field microscope image. (Reproduced with permission from ref. 53.)

Data processing and visualisation

The spectral data associated with biological ToF-SIMS analysis can be vary complex, as expected due to the complexity of the sample. Also, when combining high mass resolution and spatial resolution, sometimes with 3D analysis, the size of the data can make manipulation and visualisation difficult – it can be hard to see the wood for the trees! In order to reduce the dimensionality of the data many groups are implementing multivariate analysis methods. Previous studies have demonstrated that multivariate analysis methods can provide a useful tool for discriminating between ToF-SIMS data, either for classification of proteins based on amino acid fragment variation or the identification of microorganisms.[55,56] In the case of ToF-SIMS image analysis, such analyses can be used to improve image contrast and to identify regions of interest. Instead of working with potentially thousands of individual mass channels a small number of multivariate channels can be used to view the data. These are typically different principal components. If the multivariate analysis captures interesting looking features in the image data the components can be scrutinised in an attempt to identify the masses associated with the component.[57] Comparative studies of various pre-processing procedures for principal components analysis (PCA) along with maximum autocorrelation factor (MAF) analysis have indicated that for SIMS imaging MAF is potentially the best for reducing the number of variables required to describe the image, enhancing image contrast and recovering key spectral features, although it is more computationally intense.[58] Despite this the nature of the data can affect the outcome of the computer analysis and there still seems to be no single best case for multivariate analysis of SIMS data. A wide range of examples and discussion of approaches to multivariate data treatment for ToF-SIMS can be found in a recent two-part special edition of *Surface and Interface Analysis*.[59,60]

A further visualisation issue regarding 3D cell imaging SIMS is the possible requirement to correct for initial topography and possibly also changes in sample topography due to sputtering at different rates through different parts of the cell. If the sample is of a known uniform thickness a first approximation of the sputter rate through different areas can be made by observing the

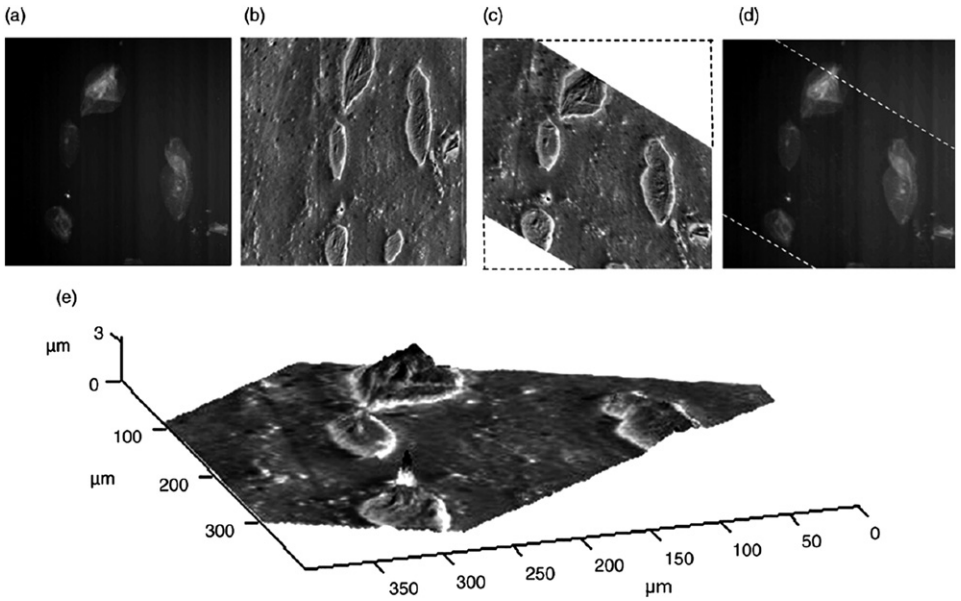

Fig. 12 Illustration of the steps for overlying topographic (AFM) and chemical (SIMS) data. AFM image (a), total secondary ion image (b), ion image following scaling and shaping using like point selection in both images (c), overlay of the reshaped ion image and the AFM image (d), and ion image 'draped' over the AFM data showing signal intensity (grey scale) and topography (*z*-axis) (e). (Reproduced with permission from ref. 46. Copyright 2008, Elsevier.)

time at each pixel that the substrate becomes continually visible. This can help in attempts to quantify signal levels as the observed secondary ion signal is proportional to the sputter yield.[61] If, however, the sample is not of homogenous thickness, the substrate will be reached at a rate dependent on both sputter rate and starting thickness. Also, when acquiring and subsequently reconstructing a 3D data set using SIMS, the cells appear to be upside down with the thicker parts of the cell penetrating the substrate. Fig. 10 panels j, k and l show the results from the 3D analysis following depth correction using the appearance of the substrate. Another method of correction is performing a topographical measurement prior to analysis, usually, although there are few examples, using atomic force microscopy (AFM) and then offsetting the SIMS data.[46,62] Fig. 12 shows an example topography correction where the SIMS signal from human cheek cells is draped over an AFM. The AFM provides the shape while the grey scale represents secondary ion signal. At present there are not enough data to predict to what extent preferential sputtering will produce artefacts in the data when using the new polyatomic beams, and work in this area is ongoing. Wucher *et al.* have illustrated that gross variations in sputter rate can exist in samples of mixed inorganic and organic composition and simple image stacking from these samples can give a distorted 3D representation without systematic pixel by pixel correction.[62] Accurate image display will be particularly important if multimodal imaging using fluorescence or spectroscopic techniques is to be performed, although the SIMS would nearly always need to be performed last due to the destructive nature of the technique.

Conclusions

Cell imaging with SIMS has reached the stage where atomic and molecular species can be routinely imaged on a sub-cellular scale. However, further validation of the technique by cross-comparison with complementary analytical methods is required before the results can be easily accepted by the biological community. There are still areas in SIMS that are not fully understood or characterised, including the role of the chemical environment or the ionisation process. Traditional dynamic SIMS and multi-isotope imaging, although limited to atomic species, have, by careful experimental design, demonstrated the ability to provide insights into biomedical and pharmacological processes.

Molecular SIMS has struggled in the past due to limitations arising from ion beam-induced damage. However, with the introduction of cluster ion beams such as C_{60} the obtainable signal has increased and 3D imaging has become a new avenue for analysis. Many pharmaceuticals are stable to bombardment with C_{60} and thus present exciting targets for ToF-SIMS analysis in cells and also tissue sections.

New developments in instrumentation look set to combine the benefits of both approaches. However, the low ionisation efficiency observed in SIMS may still limit the detection of some species at physiological levels. As described previously, methods do exist for increasing the ionisation in SIMS analysis although, as illustrated, care must be taken during interpretation of the image data following surface modification and there is no global method of laser post-ionisation. Dynamic SIMS analysts often select different ion beams for the detection of positive or negative secondary ions. The high dose of primary ions in the experiment leads to the formation of an altered layer where there is an accumulation of species from the primary ion beam. Oxygen beams are often used to enhance positive ion signals and caesium to promote the formation of negative ions. Biddulph *et al.* have experimented with coronene, $C_{24}H_{12}$, as a primary ion in an attempt to combine the sputter yield of the carbon cluster beams with increased ionisation, by protonation, of organic molecules. Unfortunately, possibly due to the relatively small amount of

hydrogen compared to the ejected species, no significant enhancement was observed.[63]

Sample preparation is a key step in the SIMS analysis and as yet there is no consensus on what the best approach maybe although the argument for frozen hydrated analysis, due to the preservation of the lifelike state, is a strong one despite the complexities and complications imposed by the ultra high vacuum requirement.

Despite the challenges SIMS can provide sub-cellular chemical-specific imaging now, and as the biological community becomes increasingly aware of the potentials of SIMS for cellular analysis, demand for the information that SIMS can provide will no doubt provide an increased impetus to investigate and overcome the remaining hurdles.

Acknowledgements

The author acknowledges the financial support of the Engineering and Physical Sciences Research Council, EPSRC, UK under grants EP/C008251 and EP/G045623/1.

References

1 J. J. Thomson, *Philos. Mag. Ser. 6*, 1910, **20**(118), 752.
2 G. H. Morrison and G. Slodzian, *Anal. Chem.*, 1975, **47**(11), 932A.
3 R. Levi-Setti, J. M. Chabala, K. Gavrilov, R. Espinose III and M. M. Le Beau, *Microsc. Res. Tech.*, 1997, **36**, 301.
4 R. Levi-Setti, K. L. Gavrilov, P. L. Strissel and R. Strick, *Appl. Surf. Sci.*, 2004, **231–232**, 479.
5 X. Zha, W. A. Ausserer and G. H. Morrison, *Cancer Res.*, 1992, **52**, 5219.
6 D. R. Lorey II, G. H. Morrison and S. Chandra, *Anal. Chem.*, 2001, **73**, 3947.
7 S. Chandra and D. R. Lorey II, *Int. J. Mass Spectrom.*, 2007, **260**, 90.
8 http://www.cameca.com/html/product_nanosims.html.
9 C. Lechene, F. Hillion, G. McMahon, D. Benson, A. M. Kleinfeld, J. P. Kampf, D. Distel, Y. Luyten, J. Bonventre, D. Hentschel, K. M. Park, S. Ito, M. Schwartz, G. Benichou and G. Slodzian, *J. Biol.*, 2006, **5**(6), 20.
10 L. A. Klerk, A. F. M. Altelaar, M. Froesch, L. A. McDonnell and R. M. A. Heeren, *Int. J. Mass Spectrom.*, 2009, **285**, 19.
11 A. G. Sostarecz, C. M. McQuaw, A. G. Ewing and N. Winograd, *J. Am. Chem. Soc.*, 2004, **126**(43), 13882.
12 M. C. Biesinger, D. J. Miller, R. R. Harbottle, F. Possmayer, S. N. McIntrye and N. O. Peterson, *Appl. Surf. Sci.*, 2006, **252**(19), 6957.
13 M. J. Baker, L. Zheng, N. Winograd, N. P. Lockyer and J. C. Vickerman, *Langmuir*, 2008, **24**(20), 11803.
14 T. L. Colliver, C. L. Brummel, I. L. Pacholski, F. D. Swanek, A. G. Ewing and N. Winograd, *Anal. Chem.*, 1997, **69**, 2225.
15 S. G. Ostrowski, C. T. Van Bell, N. Winograd and A. G. Ewing, *Science*, 2004, **305**, 71.
16 T. P. Roddy, D. M. Cannon Jr, S. G. Ostrowski, N. Winograd and A. G. Ewing, *Anal. Chem.*, 2002, **74**, 4020.
17 S. G. Ostrowski, M. E. Kurczy, T. P. Roddy, N. Winograd and A. G. Ewing, *Anal. Chem.*, 2007, **79**, 3554.
18 H. Nygren, C. Eriksson, P. Malmberg, H. Sahlin, L. Carlsson, J. Lausmaa and P. Sjövall, *Colloids Surf., B*, 2003, **30**, 87.
19 P. Sjövall, J. Lausmaa, H. Nygren, L. Carlsson and P. Malmberg, *Anal. Chem.*, 2003, **75**, 3429.
20 H. Nygren and P. Malmberg, *J. Microsc.*, 2004, **215**, 156.
21 A. F. M. Altelaar, J. Van Minnen, C. R. Jimenez, R. M. A. Heeren and S. R. Piersma, *Anal. Chem.*, 2005, **77**, 735.
22 L. A. McDonnell, S. R. Piersma, A. F. M. Alterlaar, T. H. Mize, S. L. Luxembourg, P. D. E. M. Verhaert, J. Van Minnen and R. M. A. Heeren, *J. Mass Spectrom.*, 2005, **40**, 160.
23 A. F. M. Altelaar, I. Klinkert, K. Jalink, R. P. J. De Lange, R. A. H. Adan, R. M. A. Heeren and S. R. Piersma, *Anal. Chem.*, 2006, **78**, 734.
24 M. Fartmann, C. Kriegskotte, S. Dambach, A. Wittig, W. Sauerwein and H. F. Arlinghaus, *Appl. Surf. Sci.*, 2004, **231–232**, 428.
25 H. F. Arlinghaus, C. Kriegeskotte, M. Fartmann, A. Wittig, W. Sauerwein and D. Lipinsky, *Appl. Surf. Sci.*, 2006, **252**, 6941.
26 H. H. Andersen and H. L. Bay, *J. Appl. Phys.*, 1974, **45**(2), 953.
27 K. Wittmaack, *Surf. Sci.*, 1979, **90**, 557.
28 S. S. Johar and D. A. Thompson, *Surf. Sci.*, 1979, **90**, 319.
29 M. G. Blain, S. Della-Negra, H. Joret, Y. Le Beyec and E. A. Schweikert, *Phys. Rev. Lett.*, 1989, **63**, 1625.
30 M. G. Blain, S. Della-Negra, H. Joret, Y. Le Beyec and E. A. Schweikert, *J. Vac. Sci. Technol.*, 1990, **A8**, 2265.
31 N. Davies, D. E. Weibel, P. Blenkinsopp, N. Lockyer, R. Hill and J. C. Vickerman, *Appl. Surf. Sci.*, 2003, **203–204**, 223.
32 F. Kollmer, *Appl. Surf. Sci.*, 2004, **231–232**, 153.
33 A. D. Appelhans and J. E. Delmore, *Anal. Chem.*, 1989, **61**(10), 1087.
34 F. Kotter and A. Benninghoven, *Appl. Surf. Sci.*, 1998, **133**, 47.
35 G. Gillen, in *Microbeam Analysis. Proceedings of the International Conference on Microbeam Analysis, 8–15 July 2000*, Institute of Physics Conference Series 165, Taylor & Francis Ltd, London, 2000, p. 339.
36 S. C. C. Wong, R. Hill, P. Blenkinsopp, N. P. Lockyer, D. E. Weibel and J. C. Vickerman, *Appl. Surf. Sci.*, 2003, **203–204**, 219.
37 D. E. Weibel, S. C. C. Wong, N. P. Lockyer, R. Hill, P. Blenkinsopp and J. C. Vickerman, *Anal. Chem.*, 2003, **75**, 1754.
38 B. J. Garrison and Z. Postawa, *Mass Spectrom. Rev.*, 2008, **27**, 289.
39 S. Chandra, *Appl. Surf. Sci.*, 2004, **231–232**, 467.
40 J. S. Fletcher, N. P. Lockyer, S. Vaidyanathan and J. C. Vickerman, *Anal. Chem.*, 2007, **79**, 2199.
41 W. G. Hill, N. M. Southern, B. MacIver, E. Potter, G. Apodaca, C. P. Smith and M. L. Zeidel, *Am. J. Physiol.: Renal Physiol.*, 2005, **289**, F217.
42 D. Breitenstein, C. E. Rommel, R. Mollers, J. Wegener and B. Hagenhoff, *Angew. Chem., Int. Ed.*, 2007, **46**, 5332.
43 S. Chandra, M. T. Bernius and G. H. Morrison, *Anal. Chem.*, 1986, **58**(2), 493.
44 X. A. Conlan, N. P. Lockyer and J. C. Vickerman, *Rapid Commun. Mass Spectrom.*, 2006, **20**, 1327.
45 E. A. Jones, N. P. Lockyer, J. Kordys and J. C. Vickerman, *J. Am. Soc. Mass Spectrom.*, 2007, **18**, 1559.
46 J. S. Fletcher, A. Henderson, G. X. Biddulph, S. Vaidyanathan, N. P. Lockyer and J. C. Vickerman, *Appl. Surf. Sci.*, 2008, **255**, 1264.
47 L. L. Zheng, A. Wucher and N. Winograd, *Appl. Surf. Sci.*, 2008, **255**, 816.
48 E. S. F. Berman, S. L. Fortson, K. D. Checchi, L. Wu, J. S. Felton, K. J. J. Wu and K. S. Kulp, *J. Am. Soc. Mass Spectrom.*, 2008, **19**, 1230.
49 J. Malm, D. Giannaras, M. O. Riehle, N. Gadegaard and P. Sjövall, *Anal. Chem.*, 2009, **81**, 7197.
50 D. Breitenstein, C. E. Rommel, J. Stolwijk, J. Wegener and B. Hagenhoff, *Appl. Surf. Sci.*, 2008, **255**, 1249.
51 M. C. Mony and E. Larras-Regard, *Biology of the Cell*, 1997, **89**, 199.
52 A. Carado, M. K. Passarelli, J. Kozole, J. E. Wingate, N. Winograd and A. V. Loboda, *Anal. Chem.*, 2008, **80**(21), 7921.
53 J. S. Fletcher, S. Rabbani, A. Henderson, P. Blenkinsopp, S. P. Thompson, N. P. Lockyer and J. C. Vickerman, *Anal. Chem.*, 2008, **80**, 9058.
54 A. A. Makarov, E. N. Raptakis and P. J. Derrick, *Int. J. Mass Spectrom. and Ion Processes*, 1995, **146**, 1652.
55 J. S. Fletcher, A. Henderson, R. M. Jarvis, N. P. Lockyer, J. C. Vickerman and R. Goodacre, *Appl. Surf. Sci.*, 2006, **252**(19), 6869.
56 M. S. Wagner and D. G. Castner, *Appl. Surf. Sci.*, 2004, **231–232**, 366.
57 J. L. S. Lee, I. S. Gilmore and M. P. Seah, *Surf. Interface Anal.*, 2008, **40**(1), 1.
58 B. J. Tyler, G. Rayal and D. G. Castner, *Biomaterials*, 2007, **28**(15), 2412.
59 I. S. Gilmore and M. S. Wagner, *Surf. Interface Anal.*, 2009, **41**(2), 75.
60 I. S. Gilmore and M. S. Wagner, *Surf. Interface Anal.*, 2009, **41**(8), 633.
61 A. J. Patkin, S. Chandra and G. H. Morrison, *Anal. Chem.*, 1982, **54**(14), 2507.
62 L. L. Zheng, A. Wucher and N. Winograd, *Anal. Chem.*, 2008, **80**(19), 7363.
63 G. X. Biddulph, A. M. Piwowar, J. S. Fletcher, N. P. Lockyer and J. C. Vickerman, *Anal. Chem.*, 2007, **79**, 7259.